Sisyphus optical lattice decelerator

Chun-Chia Chen (陳俊嘉), Shayne Bennetts, Rodrigo González Escudero, Florian Schreck, and Benjamin Pasquiou*
Van der Waals-Zeeman Institute, Institute of Physics, University of Amsterdam, Science Park 904, 1098XH Amsterdam, The Netherlands

(Received 18 October 2018; revised manuscript received 24 June 2019; published 1 August 2019)

Leading tests of the Standard Model, like measurements of the electron electric dipole moment or of matter-antimatter asymmetry, are built upon our ability to laser-cool atoms and molecules to ultracold temperatures. Unfortunately, laser-cooling remains limited to a minute collection of species with very specific electronic structures. To include more species, such as polyatomic molecules or exotic atoms like antihydrogen, new cooling methods are needed. Here we demonstrate a method based on Sisyphus cooling that was proposed for laser-cooling antihydrogen. In our implementation, atoms are selectively excited to an electronic state whose energy is spatially modulated by an optical lattice, and the ensuing spontaneous decay completes one Sisyphus cycle. We show that this method eliminates many constraints of traditional radiation-pressure-based approaches, while providing similar atom numbers with lower temperatures. This laser-cooling method can be instrumental in bringing new exotic species and molecules to the ultracold regime.

DOI: 10.1103/PhysRevA.100.023401

I. INTRODUCTION

Precision measurement with cold atoms and molecules is allowing us to probe the validity and limitations of the Standard Model [1,2], including searches for the electron electric dipole moment [3–5], for dark matter [6,7], and for variations in fundamental constants [8–10]. Recent breakthroughs in laser cooling, focused on using molecules with close-to-diagonal Frank-Condon factors [11–14], have been crucial enablers for many of these experiments.

Yet many of today's most exciting proposals require first extending these successes to efficiently cool new atomic and molecular species. For example, the ability to precisely compare the spectra of hydrogen with antihydrogen might shed light on one of the most important mysteries of physics today, the asymmetry between matter and antimatter. However, the ability to generate a robust trapped sample of ultracold antihydrogen [15–20] is strongly constrained by the limitations of current laser technology at 121.6 nm [21–24]. Other proposals call for ultracold samples of complex, polyatomic molecules [25–29]. While the use of radiation pressure has been wildly successful at slowing some atomic species, the need to scatter vast numbers of photons makes it difficult to apply these methods to slow species without very closed cycling transitions. Common molecules with a myriad of internal states and leaky transitions typically suffer from heavy losses. There remains a strong need for the continued development of new laser-cooling methods in order to tackle these important frontiers.

A range of approaches has been devised to achieve improved performance while relaxing constraints imposed by traditional Doppler cooling techniques. For example, rapid cycling using stimulated emission can provide stronger momentum transfer without spontaneous heating or loss from nonclosed cycling transitions. This is demonstrated in bichromatic force cooling [30,31], adiabatic rapid passage [32], and SWAP cooling [33] but it requires intense resonant light not available for some applications like at the 121.6-nm transition needed for antihydrogen. Alternatively, Sisyphus-like cooling methods [34], where kinetic energy is converted into potential energy, can function effectively even at very low excitation rates and are routinely applied to beat the Doppler temperature limit [35]. Examples of this approach include Zeeman-Sisyphus decelerators [36] and Rydberg-Stark decelerators [37,38], where a photon excitation changes the internal state, allowing a significant part of the slowing to be done by an externally applied electromagnetic field gradient.

In this work, we present a proof-of-principle demonstration of a class of proposals developed to laser-cool antihydrogen [39] and other species [40–42]. Our demonstration uses a Sisyphus-like deceleration mechanism to slow a continuous stream of strontium atoms without using radiation pressure. The method uses a one-dimensional (1D) optical lattice acting on the excited $^3P_1$ electronic state, combined with a selective excitation mechanism that transfers atoms to the lattice potential minima. We explore the performance of this method, which we call the Sisyphus optical lattice decelerator (SOLD). To compare it with traditional radiation pressure schemes we also substitute the SOLD with a Zeeman slower using the same transition as our excitation mechanism. In principle, using a deep lattice very few excitation photons can be sufficient to bring fast atoms to rest, making the SOLD a good decelerator candidate for exotic species and molecules without a closed cycling transition [11–14,25–29].

This paper is structured as follows. In Sec. II we present the working principle of the SOLD. We describe in Sec. III our implementation to slow a beam of strontium atoms and measure its performance. Section IV describes the various parameter regimes for the removal of an atom's kinetic energy, then elaborates on the SOLD efficiency in terms of the required number of scattered photons. In Sec. V we explain the

*SOLD@strontiumBEC.com

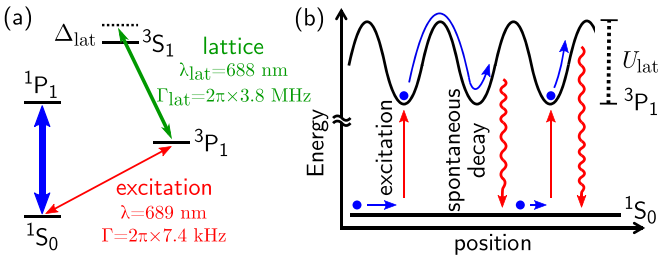

FIG. 1. SOLD working principle. (a) Relevant electronic levels of strontium and the two transitions used for excitation and optical lattice creation, both necessary for the SOLD. (b) Schematic of two typical cooling cycles, from excitation to spontaneous decay.

behavior of the excitation rate, and from this analysis we provide a simple formula for the capture velocity of this cooling method. We compare in Sec. VI the SOLD performance with typical radiation-pressure-based laser-cooling. In Sec. VII we discuss eventual limitations to the applicability of this method, and we conclude in Sec. VIII.

II. PRINCIPLE

The working principle of the SOLD relies on a three-level system coupled by two optical transitions, something ubiquitous for both atomic and molecular species. Our implementation using strontium is depicted in Fig. 1(a). An optical lattice is formed using a pair of coherent counter-propagating beams with a frequency in the vicinity of the $^3P_1$-$^3S_1$ transition. This produces a spatially modulated coupling between the $^3P_1$ and the $^3S_1$ states and thus a spatially modulated light shift on the excited $^3P_1$ state. The ground $^1S_0$ state remains essentially unaffected. By applying a laser resonant with the $^1S_0$-$^3P_1$ transition, atoms can be excited into the $^3P_1$ state, where they experience the force associated with the lattice potential [see Fig. 1(b)]. If the linewidth Γ of the $^1S_0$-$^3P_1$ intercombination line is much smaller than the lattice height $U_{lat} \gg \hbar\Gamma$, this "excitation" laser can be tuned to selectively address the bottom of the lattice sites. For a high enough velocity $v > \lambda_{lat}\Gamma$, atoms excited into $^3P_1$ will then climb a significant fraction of the lattice potential hills and lose kinetic energy before spontaneously decaying to the ground state as shown in Fig. 1(b). As atoms in $^1S_0$ propagate along the lattice axis, this cooling cycle repeats, forming a Sisyphus mechanism. By creating a very high lattice, it is theoretically possible to remove most forward kinetic energy within distances of a few lattice periods or with a single cycle, as in Rydberg-Stark decelerators [37,38]. The temperature limit for this scheme is the higher of an effective Doppler temperature depending on Γ [41], or the recoil temperature.

III. EXPERIMENTAL SETUP

To demonstrate the feasibility of the SOLD experimentally, we implement the setup shown in Fig. 2(a). We start with a magneto-optical trap (MOT) for ^{88}Sr operating in a steady-state regime on the 7.4 kHz-linewidth $^1S_0$-$^3P_1$ transition, as described in our previous work (configuration "Red MOT I" in [43]). We overlap this MOT with an optical dipole trap acting as a "transport" guide [44]. This 1D guide is $\sim$35 μK deep

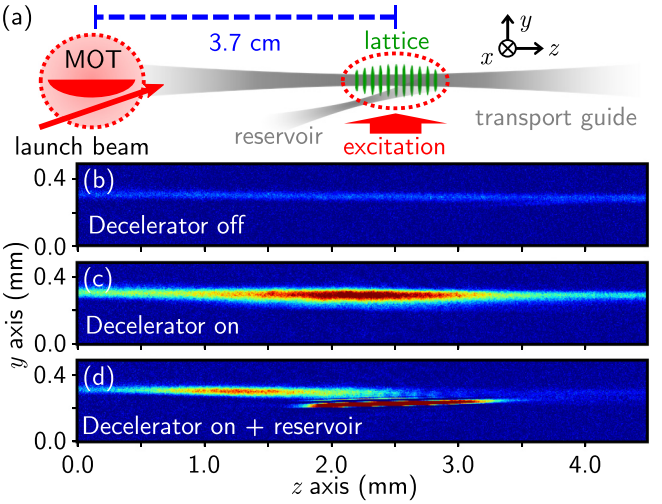

FIG. 2. (a) Side view of the setup. (b)–(d) $^1S_0$-$^1P_1$ absorption imaging pictures of the atomic beam at the decelerator location: without lattice (b), with lattice (c), and with lattice and reservoir (d).

at the MOT location and propagates horizontally along the z axis. By adding a "launch" beam resonant with the $^1S_0$-$^3P_1$ π transition and pointed at the overlap between the MOT and the transport guide, we outcouple MOT atoms into the guide with a well-controlled mean velocity ranging from 0.08 to 0.25 m s^{-1} [44]. Atoms then propagate along the guide for $\sim$3.7 cm until they reach the decelerator region.

We produce a 1D lattice potential with a pair of counter-propagating laser beams whose frequency is blue-detuned by $\Delta_{lat} \approx 2\pi \times 30$ GHz from the $^3P_1$-$^3S_1$ transition. The lattice beams cross the transport guide at the shallow angle of 6°, overlapping the atomic beam for about 3.4 mm. Excitation from the $^1S_0$ to the $^3P_1$ state is provided by illuminating the atoms from the radial direction. This is implemented using a pair of counter-propagating horizontal beams and a single vertical beam propagating upward, with $1/e^2$ diameters of 28.8 and 36 mm, respectively. These "excitation" laser beams are 15 kHz red-detuned from the π transition and their combined intensity corresponds to a saturation parameter of $\sim$1. In addition to state excitation, these beams provide an optical molasses, which brings the atoms' radial temperature to $\sim$2 μK. Importantly, we do not apply any near-resonant light capable of slowing atoms in the z axis in the absence of the SOLD optical lattice. Despite the possibility of other orientations of the excitation beams, as suggested in Ref. [39], we initially chose the configuration described above in order to demonstrate that radiation pressure is not directly involved in the slowing of atoms, and just climbing the lattice potential removes the kinetic energy.

We operate the decelerator on a guided atomic beam continuously fed by the MOT, with a homogeneous axial density across the full field of view of our imaging system [see Fig. 2(b)]. When the lattice is switched on, the density in the overlap region between the atomic and the lattice beams sharply increases, suggesting an accumulation of slowed atoms, as shown in Fig. 2(c). Without either lattice beam or with a large (160 MHz) frequency difference between the two lattice beams, this feature vanishes. Figure 2(c) also shows

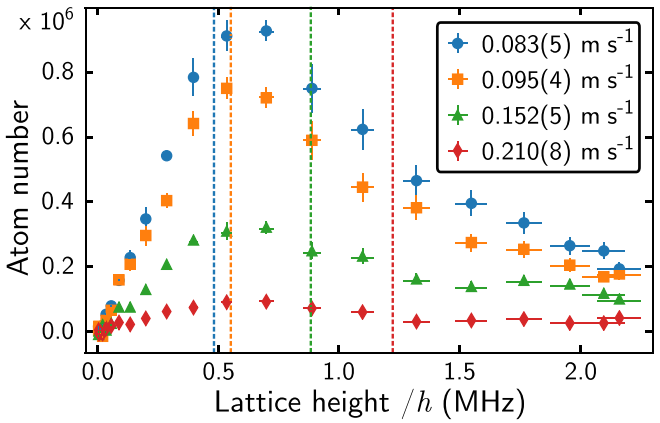

FIG. 3. SOLD efficiency. Measured steady-state number of atoms slowed by the SOLD and loaded in the reservoir, for varying lattice heights and four initial velocities. Dashed vertical lines represent the criterion of Eq. (3) for $m = 1$. Vertical error bars represent standard errors from binned data points. The origin of the horizontal error bars is described in Appendix A.

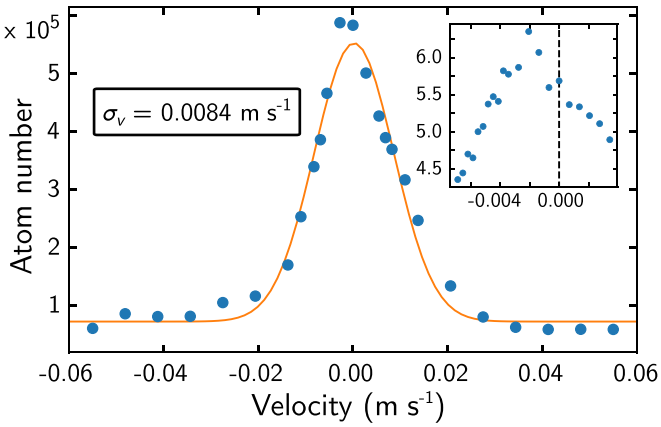

FIG. 4. Velocity selectivity of the reservoir loading, measured by varying the lattice velocity. The line is a Gaussian fit of the data with width σ_v. Inset: The same type of measurement over a much narrower velocity range, highlighting the center velocity of about $v_R \sim -0.002$ m s^{-1}.

that some atoms travel completely across the lattice region due to incomplete slowing or by diffusion. Note that our slowing mechanism is fully compatible with a steady-state apparatus, and we perform our measurements after reaching steady state.

For better characterization of the SOLD, and since we are concerned about diffusion of slowed atoms, we add a second "reservoir" dipole trap beam. This beam crosses below the transport guide at the lattice location, with an offset adjusted to allow slow atoms to pass from the guide into the reservoir while not significantly disturbing the potential landscape of the guide. With the help of the radial optical molasses, the reservoir collects and stores slowed atoms 2 mm away from the crossing. We show one example of loading into this reservoir in Fig. 2(d), which also exemplifies a means of atom extraction from our ultracold atom source. We show in Fig. 3 the measured atom number loaded into the reservoir by the SOLD. The efficiency is poor for small lattices, as not enough kinetic energy is removed before atoms leave the lattice location. For increasing lattice height, we observe a clear loading optimum, followed by a slow decrease. As we discuss in Sec. V, these two features originate from the behavior of the excitation rate to $^3P_1$.

The SOLD deceleration scheme brings atoms ultimately to zero mean velocity in the reference frame of the lattice. By applying a small frequency difference between two lattice beams, a lattice will move at a well-controlled velocity [45,46]. This implies that the SOLD can ideally decelerate or accelerate atoms to any desired velocity (see Appendix C). Here we use the moving lattice to characterize the reservoir dipole trap. The loading of this reservoir is sensitive both to the mean velocity of atoms and to the location at which they end up when reaching zero mean velocity. We characterize the velocity acceptance of the reservoir by varying the frequency difference between the two lattice beams. The loading efficiency of the reservoir depending on the lattice velocity is shown in Fig. 4. It can be fitted by a Gaussian whose width is $\sigma_v = 0.0084(4)\,\mathrm{m\,s^{-1}}$, centered at $v_R \sim -0.002\,\mathrm{m\,s^{-1}}$. This slight departure from zero velocity can be explained by the orientation of the reservoir relative to the guide, which favors the loading of atoms that move backward. The small velocity window for which the loading efficiency is substantial exemplifies the slowing effect of the SOLD.

IV. KINETIC ENERGY REGIMES AND PHOTON SCATTERING EFFICIENCY

We can understand the SOLD slowing efficiency observed in Fig. 3 with a simple semiclassical model describing its various working regimes, which depend on the relative magnitude of the atoms' kinetic energy with respect to lattice height. Consider atoms initially excited into the $^3P_1$ state at the bottom of the lattice potential. In Fig. 5(a), we plot the dependence of the average energy lost per cooling cycle E_{lost} with incoming velocity v and lattice height. For high kinetic energies compared to the lattice height $\frac{1}{2}mv^2 \gg U_{\mathrm{lat}}$, atoms travel through several lattice sites and the energy lost tends to $E_{\mathrm{lost}} \to \frac{U_{\mathrm{lat}}}{2}/(1 + (\frac{\lambda_{\mathrm{lat}}\Gamma}{4\pi v})^2)$; see Appendix B. When $v \gg \lambda_{\mathrm{lat}}\Gamma$,

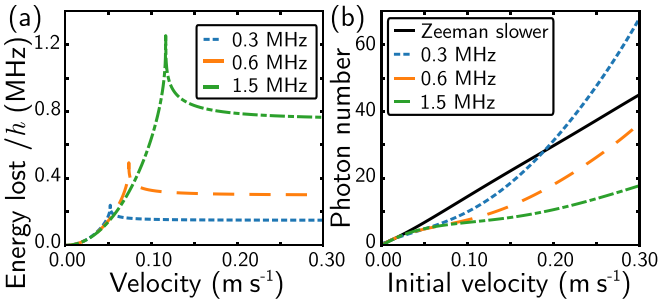

FIG. 5. Theoretical efficiency of our cooling scheme. (a) Average energy lost E_{lost} during a single cooling cycle, for varying velocities before excitation. (b) Total number of cycles and excitation photons needed for the SOLD compared with a Zeeman slower (ZS), depending on the initial velocity. The black line shows the ZS behavior, while the dotted, dashed, and dash-dotted lines represent the SOLD with various lattice heights.

the energy lost saturates to $E_{\rm lost} \to U_{\rm lat}/2$. A striking feature of Fig. 5(a) is that $E_{\rm lost}$ exhibits an efficiency peak for $\frac{1}{2}mv^2 = U_{\rm lat}$. In this case, atoms have just enough energy to climb one lattice maximum, where they spend most of their time and are thus more likely to undergo spontaneous emission. The energy lost in this regime asymptotically reaches $E_{\rm lost} \to U_{\rm lat}$ for $v \gg \lambda_{\rm lat}\Gamma$; see Appendix B. Let us note that, in contrast to Ref. [39], which relies also on a spatial modulation of Γ, the effective rate of spontaneous emission in our case is higher on lattice hills only because of the increased time atoms spend there.

Laser-cooling techniques can be benchmarked by the average number of photons that need to be scattered to slow atoms from some initial velocity to the technique's temperature limit. This is particularly relevant for species without a cycling laser-cooling transition, like most molecules [11–14,25–29], where there is a small, finite number of photons allowed to be scattered before the species decays to a dark state and is lost. Using the results of Fig. 5(a) repeated over several cycles with decreasing velocity, we calculate the number of excitation photons needed to reach a kinetic energy equivalent to a temperature below 2 μK and present it in Fig. 5(b). This temperature was arbitrarily chosen ∼4 times larger than the recoil temperature for the $^1S_0$-$^3P_1$ transition, the relevant limit in our case. For comparison with radiation-pressure-based laser-cooling methods, we also show in Fig. 5(b) the number of photons required in the case of a Zeeman slower (ZS) [47]. The SOLD always requires fewer cooling photons than the ZS for a lattice height satisfying $U_{\rm lat}/h > v/\lambda_{\rm lat}$.

V. EXCITATION RATE AND CRITICAL VELOCITY

The SOLD ability to slow atoms with high incoming velocities is strongly dependent on the excitation rate. We model this rate by solving the optical Bloch equations for a two-level system corresponding to the $^1S_0$ and $^3P_1$ states, coupled by the excitation laser with Rabi frequency Ω. The time-dependent Schrödinger–von Neumann equation for the density operator ρ is

$$\frac{d\rho}{dt} = -\frac{i2\pi}{h}[H,\ \rho] + L, \tag{1}$$

with h the Planck constant, L the usual term to account for the spontaneous emission due to Γ, and the Hamiltonian H written as

$$H = \begin{pmatrix} 0 & \Omega/2 \\ \Omega/2 & U_{\rm lat}\sin^2(2\pi\, v\, t/\lambda_{\rm lat}) \end{pmatrix}. \tag{2}$$

We numerically solve Eq. (1) with time, starting with all the population in $^1S_0$ at $t = 0$. For this calculation, we assume a constant velocity v, which is valid for $\frac{1}{2}mv^2 \gg U_{\rm lat}$. After a variable time, the (Ω, $U_{\rm lat}$, v)-dependent solution for the excited population reaches a steady state only slightly perturbed by the time-dependent detuning produced by traveling within the lattice. Averaging over this small perturbation, we get the population in the $^3P_1$ state shown in Fig. 6. Let us note that solutions for Hamiltonians similar to Eq. (2) have been analyzed before, in particular, in the frequency domain [48].

The remarkable feature in Fig. 6 is the presence of multiple resonances where there are high excitation rates. These can be explained by in-phase multiple π-over-N pulses. Indeed, only at the bottom of a lattice site is the detuning small enough to excite a significant population to $^3P_1$. While the atoms propagate from one site to the next, the distributions in $^1S_0$ and $^3P_1$ states acquire different phases. Once at the next site, further population is efficiently excited to $^3P_1$ only if the dephasing is equal to multiples of 2π, in which case the steady-state excited population is high. This behavior can be confirmed by looking at the evolution of the Bloch vector associated with ρ, displayed in Fig. 7 for two cases.

We can give a simple quantitative criterion for the positions of these excitation rate resonances. The phase accumulated

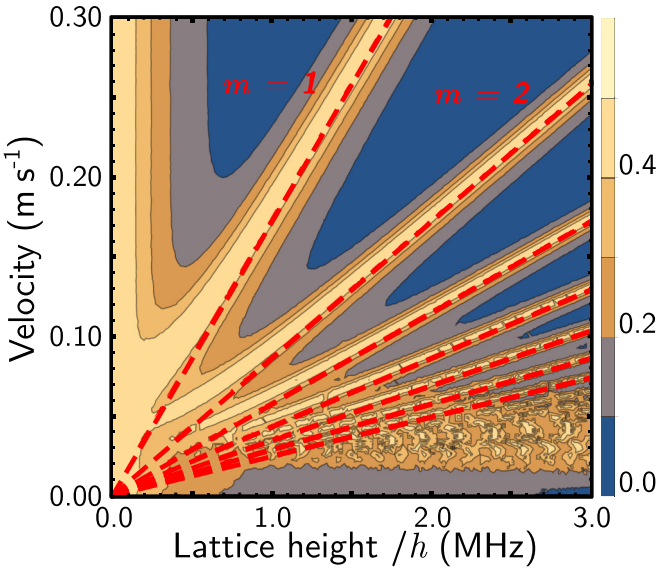

FIG. 6. Population transferred to the $^3P_1$ state depending on the lattice height and the atom velocity. For clarity, the population is calculated for a saturation parameter of the excitation transition of ∼1600 instead of the 0.1–10 typically used. Dashed red lines show the condition of Eq. (3) for $m \in \{1 \ldots 7\}$.

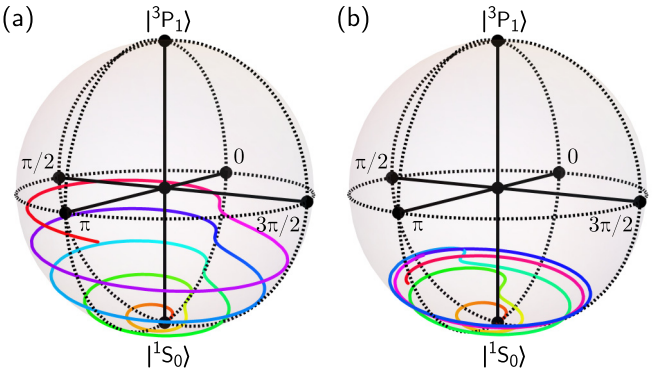

FIG. 7. Evolution of the Bloch vector on the Poincaré sphere, shortly (for five "pulses") after the application of the SOLD. Atoms begin in the $^1S_0$ state at the location of a lattice site. The saturation parameter of the excitation to $^3P_1$ is set to about 60 for clarity, and the lattice height is $h \times 600$ kHz. The velocity in (a), $v = 0.1035$ m s^{-1}, is such that the accumulated phase during the travel time between two sites is close to $\Phi = 2\pi$, while in (b), where $v = 0.09$ m s^{-1}, this condition is not met.

TABLE I. Comparison of the SOLD and the Zeeman slower (ZS). The rows list steady-state atom numbers in the reservoir (when present), fluxes, $1/e$ loading times, and reservoir radial (axial) temperatures $T_{\rm rad}$ (T_z). The various configurations are, in order, the SOLD in the transport guide, the SOLD plus the reservoir (R), the ZS plus reservoir, and the combination of both.

	SOLD	SOLD + R	ZS + R	SOLD + ZS + R
Atoms ($\times 10^6$)	0.78(01)	0.69(01)	1.87(04)	2.00(10)
Flux ($\times 10^6$ s^{-1})	0.74(04)	0.65(03)	2.11(14)	2.80(15)
Loading (ms)	705(20)	625(52)	434(43)	507(55)
$T_{\rm rad}$ (μK)		1.53(02)	1.08(04)	1.34(02)
T_z (μK)		2.30(06)	5.67(94)	2.59(10)

during the propagation through one lattice period is $\Phi = \Delta T$, with $T = \frac{\lambda_{\rm lat}}{2v}$ the propagation time and Δ the dephasing, taken as the average detuning due to the lattice, giving $\Delta = 2\pi \frac{1}{h} \frac{U_{\rm lat}}{2}$. The condition $\Phi = m \times 2\pi$ (with $m \in \mathbb{N}$) leads to the relation

$$\frac{U_{\rm lat}}{h} = m \times \frac{4v}{\lambda_{\rm lat}}. \tag{3}$$

This criterion is shown as dashed red lines for $m \in \{1, \ldots, 7\}$ in Fig. 6. Due to the high density of the lines with $m > 1$, for low incoming velocities the loading efficiency optima observed in Fig. 3 correspond mainly to fulfilling the criterion of Eq. (3) for the case $m = 1$.

Including both the average lost energy $E_{\rm lost}$ and the excitation rate, both depending on $(U_{\rm lat}, v)$, we model the behavior of the SOLD by solving classically the evolution of the atoms' velocity with time, under an effective force $F(U_{\rm lat}, v) = -\Gamma \times \rho_{^3P_1}(U_{\rm lat}, v) E_{\rm lost}(U_{\rm lat}, v)$. We reproduce qualitatively all features of the experimental data (see Appendix B). The criterion of Eq. (3) with $m = 1$ effectively dictates the capture velocity of the SOLD:

$$v_c = \frac{U_{\rm lat}\lambda_{\rm lat}}{4h}. \tag{4}$$

Let us note that, for a lattice height thus matching the atoms' velocity, the condition $U_{\rm lat}/h > v/\lambda_{\rm lat}$ given in Sec. IV is verified. Therefore, when working under nominal conditions, the SOLD requires fewer photons than standard radiation-pressure-based laser-cooling methods like the ZS.

VI. COMPARISON WITH RADIATION-PRESSURE-BASED COOLING

We now experimentally compare the SOLD performance with that of a Zeeman slower. The varying magnetic field for the ZS is provided by the existing MOT quadrupole field, whose gradient in the guide axis is 0.23 G/cm. We then add a laser beam counter-propagating to the transport guide, focused in the SOLD region and with a circular polarization set to address the high-field-seeking $^3P_1$ $m_J = -1$ state. We demonstrated in previous work that it is possible to operate a ZS on the narrow Sr intercombination line [43]. In Table I, we report a comparison between the two slowing methods. Both give similar results for fluxes and final atom numbers, with an advantage for the ZS, which we attribute mainly to the spatial selectivity of its optical excitation. However, we observe a clear difference in the final axial temperatures T_z within the reservoir, which effectively reflects the final mean velocities. For the SOLD, T_z is almost as low as the radial temperature $T_{\rm rad}$ provided by the molasses cooling, whereas T_z is 2.5 times hotter for the ZS. This is because a Zeeman slower is unable to decelerate atoms to zero velocity, as they remain somewhat resonant with ZS photons and are pushed backwards. By contrast, the final mean velocity for the SOLD is stationary in the frame of the optical lattice, which itself can be chosen arbitrarily [45,46].

An additional difference is that, since the SOLD does not rely on radiation pressure from the excitation beam to cool, it is possible to use a much broader class of transitions than for standard laser-cooling methods. It is, for example, also possible to use the ZS beam as an excitation beam that features both spatial and velocity selectivity. The lattice, now acting on atoms in $^3P_1$ $m_J = -1$, is the one charged with decelerating atoms to zero axial velocity. In the presence of both lattice and ZS beams, we observe the best number of atoms in the reservoir, while keeping the low-temperature T_z due to the SOLD (see Table I).

VII. DISCUSSION

Let us now turn to considerations for further applications of this cooling scheme. First, it is clear from Fig. 6 that, at high velocities, excitation rates are low unless the lattice height matches the conditions of Eq. (3). This can be dealt with by temporal modulation of the lattice intensity, which varies the resonance locations. Second, for lattices much higher than the transport guide depth, we observe a clear spread of the atomic beam out of the guide. This is due both to the radial anticonfinement from the blue-detuned lattice beams and the slight angle between lattice and transport beams. A red-detuned lattice could remedy this by confining the atoms radially, but this will make correctly tuning the excitation frequency dependent on the lattice intensity.

Third, if the lattice detuning $\Delta_{\rm lat}$ is insufficient, atoms in the $^3P_1$ state can be optically pumped by the lattice light to $^3S_1$. If this occurs, atoms can decay from $^3S_1$ to the metastable $^3P_0$ and $^3P_2$ states and exit the cooling cycle. Figure 8 shows, for several lattice laser detunings $\Delta_{\rm lat}$, the effect of optical pumping to $^3S_1$ depending on the lattice height. For detunings that are a few GHz away from the $^3P_1$-$^3S_1$ transition, we see a clear reduction of the maximum atom number slowed and captured in the reservoir. For detunings above 20 GHz, the efficiency seems to converge toward a unique curve, indicating no significant optical pumping. A repumping scheme such as the one used in Ref. [49] can optically pump atoms back to $^3P_1$ in a time short compared to that for the propagation of the atoms along the lattice. Alternatively, a higher detuning with a correspondingly increased intensity solves this issue. Aside from the data in Fig. 8, we operate at a lattice detuning of $\Delta_{\rm lat} \approx 2\pi \times 30$ GHz, for which optical pumping is negligible and the required optical power for the best efficiency is only 1.2 mW for each of the two 100 μm-waist beams.

Finally, the initial velocities decelerated in this proof of principle are low compared with several applications of interest, in part due to the small lattice height and deceleration

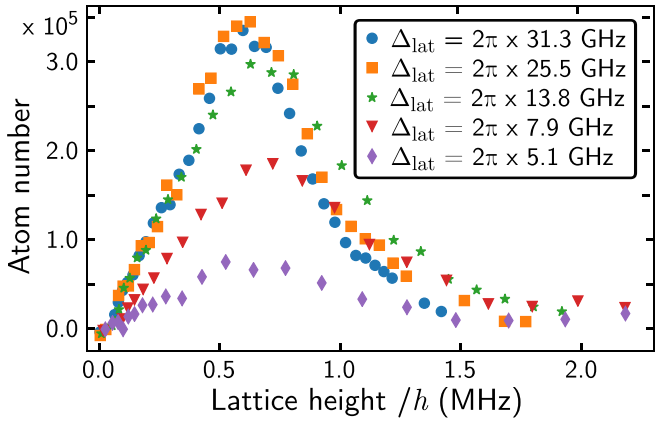

FIG. 8. Effect of optical pumping by the lattice light to the $^3S_1$ state. The data show the number of atoms loaded into the reservoir as a function of the lattice height for various detunings of the lattice laser from the $^3P_1$-$^3S_1$ transition.

region used. In the proposal of Wu *et al.* [39], the lattice is 78.5 MHz high and the capture velocity is set to $v_{c,\bar{H}} \approx 25\,\mathrm{m\,s^{-1}}$. This proposal is designed to cool trapped antihydrogen, with velocities up to $80\,\mathrm{m\,s^{-1}}$ and long interaction times including several oscillations of particles in the trap. As a comparison attempt, under these conditions it would take about 20 photon scattering events for an equivalent SOLD setup to bring antihydrogen close to the recoil limit, which, as shown in Fig. 5(b), is similar to the numbers demonstrated in this work. Let us note that one strength of this laser-cooling method is that the high optical power requirement is on the lattice transition and not on the, far more technologically challenging, 121.6 nm excitation transition.

VIII. CONCLUSION

To summarize, we experimentally demonstrate a Sisyphus-like deceleration mechanism to slow and cool strontium atoms without using radiation pressure. Our work validates a class of proposals developed for laser-cooling antihydrogen [39] and other species [40–42]. We characterize the SOLD technique in the steady-state regime both experimentally and theoretically. We compare the SOLD with a typical radiation-pressure-based scheme (Zeeman slower) and find similar atom numbers but lower axial temperatures. By combining both techniques, we benefit from the ZS spatial and velocity selectivity and improved SOLD end temperatures. We also consider some improvements and applications to the case of antihydrogen.

Using the SOLD method requires only three easily met conditions: a three-level system, selective excitation in a lattice with $U_{\mathrm{lat}} \gg \hbar\Gamma$, and an initial velocity satisfying $v > \lambda_{\mathrm{lat}}\Gamma$. Such simple requirements can be fulfilled by many systems where laser-cooling to the ultracold regime remains a challenge. Already, recent independent work has shown similar Sisyphus cooling effects in optical tweezers [50], and adapting the present laser-cooling method to new exotic species and (polyatomic) molecules [11–14,25–29] is the next logical step. Furthermore, by careful choice of the time sequence for the lattice velocity and intensity, a pulsed version of the SOLD could bring an atom wave packet to any desired velocity while scattering only a handful of photons.

ACKNOWLEDGMENTS

B.P. thanks the NWO for funding through Veni Grant No. 680-47-438. We thank the NWO for funding through Vici Grant No. 680-47-619 and the European Research Council (ERC) for funding under Project No. 615117 QuantStro. This project has received funding from the European Union's Horizon 2020 research and innovation program under Grant Agreement No. 820404 (iqClock project). C.-C.C. thanks the MOE Technologies Incubation Scholarship from the Taiwan Ministry of Education for support.

APPENDIX A: LATTICE HEIGHT DETERMINATION

We need an accurate determination of the lattice height to characterize the SOLD. The potential of a 1D lattice acting on the $^3P_1$ state depends on its dynamic dipole polarizability α. In the two-level approximation, valid here because the lattice laser detuning Δ_{lat} is only a few tens of GHz, the polarizability is given by

$$\alpha \approx \frac{3\epsilon_0\lambda_{\mathrm{lat}}^3}{8\pi^2}\frac{\Gamma_{\mathrm{eff}}}{\Delta_{\mathrm{lat}}}, \tag{A1}$$

where ϵ_0 is the vacuum permittivity. The effective rate $\Gamma_{\mathrm{eff}} = \eta A_{^3P_1-{}^3S_1}$ is the effective transition rate for the $5s5p\,^3P_1$-$5s6s\,^3S_1$ transition, with $\eta = 1/2$ due to the lattice laser polarization. The relative uncertainties of the parameters contributing to the determination of the lattice height are listed in Table II. All parameters contributing to the lattice height and their uncertainties are determined experimentally, except for $A_{^3P_1\text{-}^3S_1}$ that we derive from the literature in the following manner.

The branching ratios from the $^3S_1$ state to the three $5s5p\,^3P_J$ states can be calculated taking into account the fine-structure splitting that produces frequency-dependent correction factors. The resulting branching ratios are $^3S_1$ to $(^3P_0, {}^3P_1, {}^3P_2) = (12.02\,\%, 34.71\,\%, 53.27\,\%)$. The transition rate for $5s5p\,^3P_0$–$5s6s\,^3S_1$ was precisely determined experimentally and theoretically in Refs. [51] and [52]. By scaling this known transition according to the branching ratios, we arrive at a transition rate $A_{^3P_1\text{-}^3S_1} = 2.394(24) \times 10^7\,s^{-1}$.

APPENDIX B: SOLD MODEL

Here we give a description of our model of the SOLD that is an extended version of the description given in the text.

TABLE II. Relative uncertainties on the relevant parameters used to calculate the lattice height for the $^3P_1$ state.

	Uncertainty
Lattice beam power	±3.0 %
Lattice beam waist	±1.4 %
Lattice frequency detuning Δ_{lat}	±0.1 %
Total transition rate $A_{^3P_J\text{-}^3S_1}$	±1.0 %
Total uncertainty	±4.2 %

In order to model our cooling scheme in an insightful way, we split the problem into two parts: the average energy lost per cooling cycle and the excitation rate. The excitation rate has been described extensively in the text. As for the energy lost, we give more details below. We then use both energy lost and excitation rate results to simulate the time evolution of the atoms' velocity.

1. Energy lost

We begin with a study of the energy lost due to the presence of the lattice. We assume that the atoms are excited into the $^3P_1$ state at the bottom of the lattice and we solve the differential equation for the motion $z(t)$ along the lattice propagation axis,

$$\frac{1}{2}mv_0^2 = U_{\rm lat}\sin^2 k_{\rm lat}z + \frac{1}{2}m\left(\frac{dz}{dt}\right)^2, \quad z(t=0)=0, \quad \text{(B1)}$$

with m and v_0 being, respectively, the mass and the initial velocity of the atom. $U_{\rm lat}$ is the lattice depth and $k_{\rm lat} = \frac{2\pi}{\lambda_{\rm lat}}$ is the wave vector of the lattice light with wavelength $\lambda_{\rm lat}$. The solution of this equation can be written in terms of the Jacobi amplitude J_A:

$$z(t) = \frac{1}{k_{\rm lat}}J_A\left(k_{\rm lat}v_0\,t, \frac{2U_{\rm lat}}{mv_0^2}\right). \quad \text{(B2)}$$

Since the process relies on spontaneous emission towards $^1S_0$, we determine the average energy lost $E_{\rm lost}(U_{\rm lat}, v_0)$ by integrating the lattice height explored for a duration set by the natural linewidth Γ of the $^1S_0$-$^3P_1$ transition,

$$E_{\rm lost} = \Gamma\int_0^\infty e^{-\Gamma t}\,U_{\rm lat}\sin^2(k_{\rm lat}z(t))\,dt. \quad \text{(B3)}$$

In Fig. 5(a), we show the evolution of $E_{\rm lost}$ for several lattice heights and depending on the incoming velocity. We observe that for high incoming kinetic energies compared to the lattice height $\frac{1}{2}mv_0^2 \gg U_{\rm lat}$, the energy lost $E_{\rm lost}$ saturates. In this case, atoms travel through several lattice sites, and their propagation tends to $z(t) \to \frac{1}{k_{\rm lat}}J_A(k_{\rm lat}v_0\,t, 0) = v_0\,t$. Equation (B3) gives the relation $E_{\rm lost} \to \frac{U_{\rm lat}}{2}/(1+(\frac{\Gamma}{2k_{\rm lat}v_0})^2)$. In our experiment $v_0 \gg \lambda_{\rm lat}\Gamma$, so the average energy lost saturates to $U_{\rm lat}/2$. One striking feature of Fig. 5(a) is that the energy lost exhibits a sharp resonance for $\frac{1}{2}mv_0^2 = U_{\rm lat}$, where cooling is the most efficient. In this case, atoms have just enough energy to climb on top of the first lattice hill, so they spend most of their time at this location, which makes them more likely to spontaneously emit there and therefore to lose most of their kinetic energy. Indeed, the explored lattice height becomes $U(t) \to U_{\rm lat}\tanh^2(k_{\rm lat}v_0\,t)$, which for $v_0 \gg \lambda_{\rm lat}\Gamma$ gives an average energy lost reaching asymptotically $E_{\rm lost} \to U_{\rm lat}$.

2. Overall evolution

In order to model the complete behavior of the SOLD, we solve classically the evolution of the atoms' velocity v with time, under an effective force $F(U_{\rm lat}, v) = -\Gamma \times \rho_{^3P_1}(U_{\rm lat}, v)\,E_{\rm lost}(U_{\rm lat}, v)$. We carry out this calculation for a packet of atoms whose velocity distribution follows a (1D) Boltzmann distribution corresponding to the temperature of our MOT of 6 μK summed with an offset corresponding to the measured mean velocity given by the launch beam. The capture probability in our reservoir is determined by the velocity-dependent efficiency extracted from the measurement shown in Fig. 4, corresponding to a Gaussian function with a width $\sigma_v = 0.0084\,\mathrm{m\,s^{-1}}$. We thus simulate the time evolution of the loaded population in the reservoir depending on the lattice height, for the four mean starting velocities shown in Fig. 3. In Fig. 9 we compare the results from this model with our experimental data.

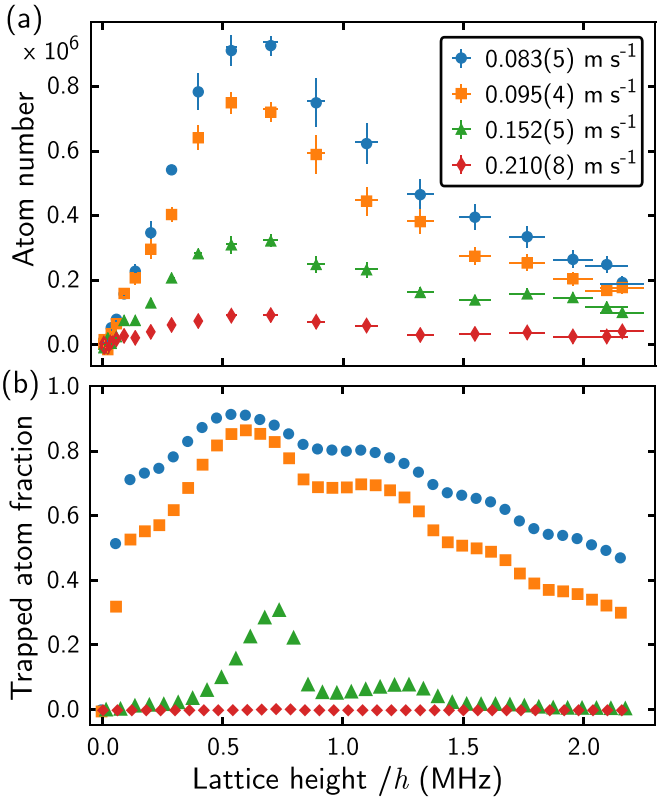

FIG. 9. Comparison between (a) the experimental data shown in Fig. 3 and (b) the results of the theoretical model (see text) for the same initial mean velocities.

We see a good qualitative agreement concerning the overall behavior with both the lattice height and the starting mean velocity. In particular, the locations of the optima of loading efficiency are well reproduced by our model. These correspond to the case when the starting mean velocity v_0 verifies the criterion of Eq. (3) (with $m = 1$). Indeed, in that case atoms are efficiently excited to the $^3P_1$ state and typically lose a significant amount of energy $U_{\rm lat}/2$. After spontaneous emission, their velocity is much lower and atoms are in the $(U_{\rm lat}, v)$ region where the density of lines for $m \geqslant 2$ is high. They are therefore very likely to keep decelerating efficiently. On the contrary, for a high velocity v_0, in the region $0 \ll \frac{U_{\rm lat}}{h} \ll \frac{4v_0}{\lambda_{\rm lat}}$, atoms will not get excited to $^3P_1$. Our model is thus able to estimate the capture velocity v_c of the SOLD, which is given by

$$v_c = \frac{U_{\rm lat}\lambda_{\rm lat}}{4h}. \quad \text{(B4)}$$

Let us note that our model makes several approximations. Indeed the results of the calculations shown in Fig. 9(b)

are given for one particular evolution time, $t = 1.4$ ms, that has been chosen for the best match with the steady-state experimental data. Since no decay mechanism has been added in the model, the final loading would be with unity efficiency. This chosen deceleration time is rather short, because in this case the saturation parameter of the $^1S_0$-$^3P_1$ transition is set to $\sim$320, for which the calculations suffer fewer numerical errors compared to more realistic, lower saturation parameters. Nonetheless, the simulations always exhibit the same overall behavior no matter the value of the saturation parameter. Another limitation of our model is that no selection criteria have been chosen for the position of atoms, whereas they must be in the vicinity of the crossing between the transport guide and the reservoir to be loaded. Similarly, atoms expelled from the guide by the barrier formed by the blue-detuned lattice and the effects of the lattice's slight angle with the guide are not taken into account. Finally, the constant-velocity approximation made when solving the optical Bloch equations is not valid for $\frac{1}{2}mv^2 \leqslant U_{\mathrm{lat}}$. To obtain a better quantitative agreement, a more advanced theoretical study would be required [53].

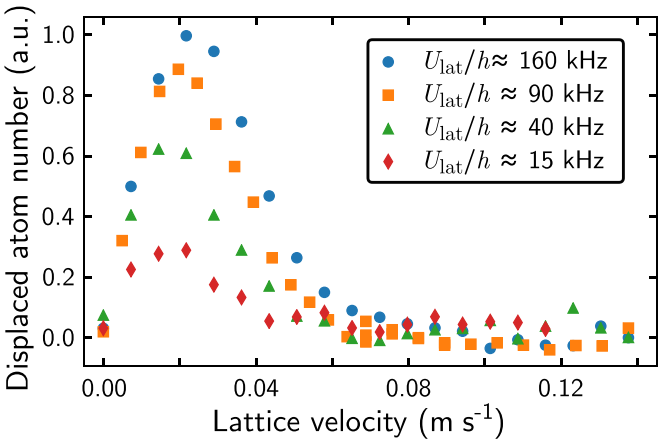

FIG. 10. Acceleration of a stationary strontium cloud by a moving lattice, for various lattice heights. The abscissa gives the lattice velocity, and the ordinate, in arbitrary units, is proportional to the fraction of atoms in the moving frame measured after 100 μs of acceleration followed by 20 ms of evolution.

APPENDIX C: SISYPHUS OPTICAL LATTICE ACCELERATOR

The SOLD deceleration scheme brings atoms ultimately to zero mean velocity in the reference frame of the lattice. By applying a small frequency difference between two lattice beams, a lattice will move at a well-controlled velocity. This implies that the SOLD can ideally decelerate or accelerate atoms to any desired velocity. We test this using a 1.53(2)-μK stationary cloud produced by loading a MOT into a dipole trap, at the location of the lattice. We shine both lattice and excitation light onto this cloud for 100 μs and, after 20 ms, observe the number of atoms in a displaced cloud corresponding to the moving lattice frame. The results are shown in Fig. 10. We observe an increase in the displaced fraction with lattice height, which we attribute to the increase in energy $\sim U_{\mathrm{lat}}/2$ given to the atoms for each scattering event. We also observe an optimal lattice velocity for a given lattice height, which roughly corresponds to our model criterion of Eq. (3) with $m = 1$. The variation in the location of these efficiency peaks is more visible in Fig. 10 than in Fig. 3, because here the SOLD is pulsed for a short duration instead of operating in the steady-state regime, so the effects of each resonance corresponding to Eq. (3) are more pronounced. Note that due to the initial size of the cloud and its location with respect to the lattice, our estimation of the effective lattice depth is much rougher than for the data in Fig. 3.

[1] M. S. Safronova, D. Budker, D. DeMille, D. F. J. Kimball, A. Derevianko, and C. W. Clark, Rev. Mod. Phys. **90**, 025008 (2018).
[2] D. DeMille, Phys. Today **68**(12), 34 (2015).
[3] J. J. Hudson, D. M. Kara, I. J. Smallman, B. E. Sauer, M. R. Tarbutt, and E. A. Hinds, Nature **473**, 493 (2011).
[4] J. Baron, W. C. Campbell, D. DeMille, J. M. Doyle, G. Gabrielse, Y. V. Gurevich, P. W. Hess, N. R. Hutzler, E. Kirilov, I. Kozyryev *et al.* (ACME Collaboration), Science **343**, 269 (2013).
[5] W. B. Cairncross, D. N. Gresh, M. Grau, K. C. Cossel, T. S. Roussy, Y. Ni, Y. Zhou, J. Ye, and E. A. Cornell, Phys. Rev. Lett. **119**, 153001 (2017).
[6] P. Wcisło, P. Ablewski, K. Beloy, S. Bilicki, M. Bober, R. Brown, R. Fasano, R. Ciuryło, H. Hachisu, T. Ido *et al.*, Sci. Adv. **4**, eaau4869 (2018).
[7] P. Wcisło, P. Morzyński, M. Bober, A. Cygan, D. Lisak, R. Ciuryło, and M. Zawada, Nat. Astron. **1**, 0009 (2016).
[8] C. J. A. P. Martins, Rep. Prog. Phys. **80**, 126902 (2017).
[9] R. M. Godun, P. B. R. Nisbet-Jones, J. M. Jones, S. A. King, L. A. M. Johnson, H. S. Margolis, K. Szymaniec, S. N. Lea, K. Bongs, and P. Gill, Phys. Rev. Lett. **113**, 210801 (2014).
[10] J.-P. Uzan, Rev. Mod. Phys. **75**, 403 (2003).
[11] J. F. Barry, D. J. McCarron, E. B. Norrgard, M. H. Steinecker, and D. DeMille, Nature **512**, 286 (2014).
[12] L. Anderegg, B. L. Augenbraun, E. Chae, B. Hemmerling, N. R. Hutzler, A. Ravi, A. Collopy, J. Ye, W. Ketterle, and J. M. Doyle, Phys. Rev. Lett. **119**, 103201 (2017).
[13] A. L. Collopy, S. Ding, Y. Wu, I. A. Finneran, L. Anderegg, B. L. Augenbraun, J. M. Doyle, and J. Ye, Phys. Rev. Lett. **121**, 213201 (2018).
[14] S. Truppe, H. J. Williams, M. Hambach, L. Caldwell, N. J. Fitch, E. A. Hinds, B. E. Sauer, and M. R. Tarbutt, Nat. Phys. **13**, 1173 (2017).
[15] G. B. Andresen, M. D. Ashkezari, M. Baquero-Ruiz, W. Bertsche, P. D. Bowe, E. Butler, C. L. Cesar, S. Chapman, M. Charlton, A. Deller *et al.*, Nature **468**, 673 (2010).
[16] G. Gabrielse, R. Kalra, W. S. Kolthammer, R. McConnell, P. Richerme, D. Grzonka, W. Oelert, T. Sefzick, M. Zielinski, D. W. Fitzakerley *et al.* (ATRAP Collaboration), Phys. Rev. Lett. **108**, 113002 (2012).

[17] M. Ahmadi, B. X. R. Alves, C. J. Baker, W. Bertsche, E. Butler, A. Capra, C. Carruth, C. L. Cesar, M. Charlton, S. Cohen *et al.*, Nature **541**, 506 (2017).
[18] M. Ahmadi, B. X. R. Alves, C. J. Baker, W. Bertsche, E. Butler, A. Capra, C. Carruth, C. L. Cesar, M. Charlton, S. Cohen *et al.*, Nature **548**, 66 (2017).
[19] M. Ahmadi, B. X. R. Alves, C. J. Baker, W. Bertsche, A. Capra, C. Carruth, C. L. Cesar, M. Charlton, S. Cohen, R. Collister *et al.*, Nature **561**, 211 (2018).
[20] N. Masuhara, J. M. Doyle, J. C. Sandberg, D. Kleppner, T. J. Greytak, H. F. Hess, and G. P. Kochanski, Phys. Rev. Lett. **61**, 935 (1988).
[21] G. Gabrielse, B. Glowacz, D. Grzonka, C. D. Hamley, E. A. Hessels, N. Jones, G. Khatri, S. A. Lee, C. Meisenhelder, T. Morrison *et al.*, Opt. Lett. **43**, 2905 (2018).
[22] K. S. E. Eikema, J. Walz, and T. W. Hänsch, Phys. Rev. Lett. **86**, 5679 (2001).
[23] I. D. Setija, H. G. C. Werij, O. J. Luiten, M. W. Reynolds, T. W. Hijmans, and J. T. M. Walraven, Phys. Rev. Lett. **70**, 2257 (1993).
[24] P. H. Donnan, M. C. Fujiwara, and F. Robicheaux, J. Phys. B **46**, 025302 (2013).
[25] I. Kozyryev and N. R. Hutzler, Phys. Rev. Lett. **119**, 133002 (2017).
[26] I. Kozyryev, L. Baum, K. Matsuda, and J. M. Doyle, ChemPhysChem **17**, 3641 (2016).
[27] T. A. Isaev and R. Berger, Phys. Rev. Lett. **116**, 063006 (2016).
[28] B. K. Stuhl, B. C. Sawyer, D. Wang, and J. Ye, Phys. Rev. Lett. **101**, 243002 (2008).
[29] I. Kozyryev, L. Baum, K. Matsuda, B. L. Augenbraun, L. Anderegg, A. P. Sedlack, and J. M. Doyle, Phys. Rev. Lett. **118**, 173201 (2017).
[30] J. Söding, R. Grimm, Y. B. Ovchinnikov, P. Bouyer, and C. Salomon, Phys. Rev. Lett. **78**, 1420 (1997).
[31] I. Kozyryev, L. Baum, L. Aldridge, P. Yu, E. E. Eyler, and J. M. Doyle, Phys. Rev. Lett. **120**, 063205 (2018).
[32] X. Miao, E. Wertz, M. G. Cohen, and H. Metcalf, Phys. Rev. A **75**, 011402(R) (2007).
[33] M. A. Norcia, J. R. K. Cline, J. P. Bartolotta, M. J. Holland, and J. K. Thompson, New J. Phys. **20**, 023021 (2018).
[34] J. Dalibard and C. Cohen-Tannoudji, J. Opt. Soc. Am. B **6**, 2023 (1989).
[35] P. D. Lett, R. N. Watts, C. I. Westbrook, W. D. Phillips, P. L. Gould, and H. J. Metcalf, Phys. Rev. Lett. **61**, 169 (1988).
[36] N. J. Fitch and M. R. Tarbutt, ChemPhysChem **17**, 3609 (2016).
[37] S. D. Hogan and F. Merkt, Phys. Rev. Lett. **100**, 043001 (2008).
[38] S. D. Hogan, C. Seiler, and F. Merkt, Phys. Rev. Lett. **103**, 123001 (2009).
[39] S. Wu, R. C. Brown, W. D. Phillips, and J. V. Porto, Phys. Rev. Lett. **106**, 213001 (2011).
[40] R. Taïeb, R. Dum, J. I. Cirac, P. Marte, and P. Zoller, Phys. Rev. A **49**, 4876 (1994).
[41] V. V. Ivanov and S. Gupta, Phys. Rev. A **84**, 063417 (2011).
[42] V. V. Ivanov, Opt. Commun. **324**, 258 (2014).
[43] S. Bennetts, C.-C. Chen, B. Pasquiou, and F. Schreck, Phys. Rev. Lett. **119**, 223202 (2017).
[44] C.-C. Chen, S. Bennetts, R. González Escudero, B. Pasquiou, and F. Schreck, arXiv:1907.02793 (2019).
[45] M. Ben Dahan, E. Peik, J. Reichel, Y. Castin, and C. Salomon, Phys. Rev. Lett. **76**, 4508 (1996).
[46] S. R. Wilkinson, C. F. Bharucha, K. W. Madison, Q. Niu, and M. G. Raizen, Phys. Rev. Lett. **76**, 4512 (1996).
[47] W. D. Phillips and H. Metcalf, Phys. Rev. Lett. **48**, 596 (1982).
[48] C. S. E. van Ditzhuijzen, A. Tauschinsky, and H. B. van Linden van den Heuvell, Phys. Rev. A **80**, 063407 (2009).
[49] T. P. Dinneen, K. R. Vogel, E. Arimondo, J. L. Hall, and A. Gallagher, Phys. Rev. A **59**, 1216 (1999).
[50] A. Cooper, J. P. Covey, I. S. Madjarov, S. G. Porsev, M. S. Safronova, and M. Endres, Phys. Rev. X **8**, 041055 (2018).
[51] M. S. Safronova, S. G. Porsev, U. I. Safronova, M. G. Kozlov, and C. W. Clark, Phys. Rev. A **87**, 012509 (2013).
[52] T. Nicholson, S. Campbell, R. Hutson, G. Marti, B. Bloom, R. McNally, W. Zhang, M. Barrett, M. Safronova, G. Strouse *et al.*, Nat. Commun. **6**, 6896 (2015).
[53] G. Grynberg and C. Robilliard, Phys. Rep. **355**, 335 (2001).